ACS APPLIED BIO MATERIALS
Article
Cite This: ACS Appl. Bio Mater. XXXX, XXX, XXX−XXX
www.acsabm.org

A Bismuth Metal−Organic Framework as a Contrast Agent for X-ray Computed Tomography

Lee Robison,[†,#] Lin Zhang,[†,#,‡] Riki J. Drout,[†] Peng Li,[†] Chad R. Haney,[§] Anlil Brikha,[§] Hyunho Noh,[†] B. Layla Mehdi,[⊥] Nigel D. Browning,[⊥] Vinayak P. Dravid,[∥] Qun Cui,[‡] Timur Islamoglu,[†] and Omar K. Farha*[,†]

[†]International Institute of Nanotechnology, Department of Chemistry, Northwestern University, 2145 Sheridan Road, Evanston, Illinois 60208-3113, United States

[‡]College of Chemical Engineering, Nanjing Tech University, 5 Xinmofan Road, Nanjing 210009, China

[§]Center for Advanced Molecular Imaging, Northwestern University, 2145 Sheridan Road, Evanston, Illinois 60208-3113, United States

[⊥]School of Engineering, University of Liverpool, Liverpool, United Kingdom

[∥]Department of Materials Science and Engineering, Northwestern University, Evanston, Illinois 60208, United States

Supporting Information

ABSTRACT: A new bismuth metal−organic framework (MOF), bismuth-NU-901 (Bi-NU-901), featuring the *scu* topology and a pore with a diameter of ∼11 Å, was solvothermally synthesized, and its use as an X-ray computed tomography (CT) contrast agent was tested. X-ray CT is a common diagnostic method used in the medical field. Inside the body, contrast media enhance the distinction between tissues and organs of similar density. Bi-NU-901 consists of eight connected Bi_6 nodes and tetratopic 1,3,5,8-(*p*-benzoate)pyrene linkers (TBAPy). Numerous material characterization studies including powder X-ray diffraction (PXRD), scanning transmission electron microscopy (STEM), and DFT pore size distribution support the *scu* structure. Additionally, given the framework's high density of nontoxic heavy atoms, Bi-NU-901 was evaluated as an X-ray computed tomography (CT) agent. Importantly, *in vitro* studies revealed this new bismuth MOF demonstrates ∼7 times better contrast intensity compared to a zirconium MOF featuring the same topology and ∼14 times better contrast than a commercially available CT contrast agent. These results suggest bismuth MOFs may be promising CT contrast agents.

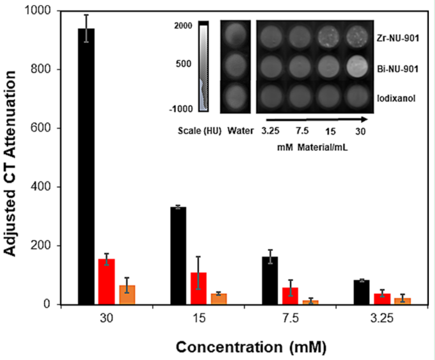

KEYWORDS: *metal−organic frameworks, contrast agent, bismuth, X-ray computed tomography*

INTRODUCTION

X-ray computed tomography (CT) allows for visualization of internal structures such as the liver, lungs, bone, cardiovascular system, and gastrointestinal system.[1] In the United States, more than 68 million clinical CT scans are undertaken every year.[2]

To be feasible for clinical use, a CT contrast agent must require the lowest dose possible, produce the maximum contrast between the tissue of interest and background scattering events, and be minimally toxic to patients.[3] Commercially sold agents are molecules composed of either iodine or barium. Unfortunately, the most widely used CT contrast agents often display only two of these three desirable characteristics. For instance, iodixanol, sold under the brand name Visipaque, obligates a dose volume delivering ∼16 g of iodine to the patient.[3] Such high doses of iodine have been known to induce immediate allergic reaction and/or cardiac, endocrine, and renal complications.[4−7] Similarly, typically administered doses of barium-based contrast agents such as VoLumen deliver ∼0.7 g of barium, and possible side effects include allergic reaction and mild to severe stomach cramping and/or diarrhea.[8] The ability of a material to attenuate X-rays and to act as a CT contrast agent can be determined by considering the mass absorption coefficient, μ, determined using eq 1.

$$\mu \approx \frac{\rho Z^4}{AE^3} \qquad (1)$$

In this equation, ρ is the material density; A is the atomic mass; Z is the atomic number, and E is the energy of the X-ray beam entering the sample.[3] The Z^4 term significantly enhances the area of interest as compared to the surrounding organs, which is largely due to the photoelectric effect. Given this fact, one can infer the use of iodine and barium CT agents is based on

Received: December 4, 2018
Accepted: February 1, 2019

DOI: 10.1021/acsabm.8b00778
ACS Appl. Bio Mater. XXXX, XXX, XXX−XXX

their ease of synthesis and cost instead of their performance in attenuating X-rays.[9]

The element bismuth ($Z = 83$) is the largest nonradioactive and synthetically accessible element on the periodic table. Its atomic number yields better X-ray attenuation over both iodine and barium. Additionally, bismuth is known to be one of the safest heavy elements to humans because of its low solubility,[10] with a recent clinical trial reporting no safety concerns for patients administered 1680 mg of Bi^{3+}/day to fight *Helicobacter pylori* infections.[11] Bismuth nanoparticles,[12,13] bismuth−carbon nanotubes,[14] and bismuth polymers[15,16] have shown promising results in CT imaging applications.

Recently, several different categories of nanomaterials for next-generation CT contrast agents have been investigated, namely, inorganic metal nanoparticles,[17−23] lipid-based structures,[24−26] and polymer-based composite materials.[27,28] Metal−organic frameworks (MOFs) are porous nanomaterials made of metal nodes and multitopic organic linkers which assemble through coordination bonds into multidimensional periodic lattices.[29] The vast assortment of inorganic nodes and organic ligands has yielded MOFs with diverse chemical functionalities and topologies. Given their crystallinity, porosity, and synthetic tunability, MOFs have been studied for applications such as separation,[30] storage,[30,31] drug delivery,[32−34]catalysis,[35] and CT contrast agents,[36] among others. Their noteworthy chemical and thermal stability has led to their use for many biologically relevant applications.[37−39] Each part of a MOF, the metal node and the organic linker, can be tuned independently to add specific functionality to the structure.[40,41] Additionally, the cavities and/or channels of metal−organic frameworks can be utilized to encapsulate different molecules of biomedical interest.[42]

The MOF, NU-901, is comprised of $Zr_6(\mu_3\text{-OH})_4(\mu_3\text{-O})_4(OH_2)_4$ nodes and tetratopic 1,3,6,8-tetrakis(*p*-benzoate)pyrene (TBAPy) linkers.[43] This framework's robust chemical and thermal stability[44] inspired us to investigate an isostructural bismuth-based analogue for its ability to act as a strong candidate for a new CT contrast agent. The porosity of MOFs is a unique feature over other potential CT contrast materials, as MOFs can encapsulate additional molecules, which may accommodate the development of future theranostics[45] or dual-function biomaterials.[37] Previously, in the literature, there are only five papers which report bismuth-based MOFs having permanent porosity, as demonstrated by nitrogen isotherm experiments. Of these five MOF materials, none have been studied for their use as possible contrast media.[46−50] In this manuscript, we report a bismuth cluster MOF, Bi-NU-901, and explore its use as contrast media for X-ray computed tomography (Figure 1).

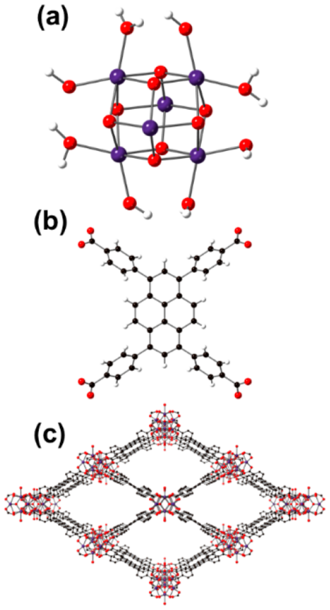

Figure 1. Bi-NU-901 is comprised of (a) Bis_6 metal nodes and (b) 1,3,6,8-tetrakis(*p*-benzoate)pyrene linkers and exhibits the (c) *scu* topology.

METHODS AND MATERIALS

Materials. The starting chemical reagents bismuth(III) nitrate pentahydrate (Sigma-Aldrich, 99.99%), anhydrous *N*,*N*′-dimethylformamide (Aldrich, 99.8%, noted DMF), reagent alcohol (Sigma-Aldrich, <0.0005% water, noted ethanol), trifluoroacetic acid (Sigma-Aldrich, ReagentPlus, 99%, noted TFA), iodixanol (Sigma-Aldrich), barium sulfate (Sigma-Aldrich, 99.99%), 10X phosphate-buffered saline (Sigma-Aldrich), bismuth standard for ICP (Sigma-Aldrich), and zirconium standard for ICP (Sigma-Aldrich) are commercially available and have been used without any further purification. The ligand 1,3,6,8-tetrakis(*p*-benzoic acid)pyrene (H_4TBAPy) was synthesized according to a published procedure.[51]

Synthesis of Bi-NU-901. Reaction of 1,3,6,8-tetrakis(*p*-benzoic acid)pyrene (H_4TBAPy) with $Bi(NO_3)_3\cdot 5H_2O$ in a solution of *N*,*N*-dimethylformamide (DMF), ethanol, and trifluoroacetic acid (TFA) at 100 °C for 8 h yields a yellow powder of Bi-NU-901. The bismuth salt solution was prepared by mixing $Bi(NO_3)_3\cdot 5H_2O$ (80 mg, 0.16 mmol) and TFA (200 μL, 5.88 mmol) in DMF (10 mL) in a 6-dram vial. The solution was heated at 100 °C for 1 h. Upon cooling to room temperature, H_4TBAPy linker (40 mg, 0.06 mmol) and additional DMF (10 mL) were added to the bismuth salt solution. The resulting pale-yellow solution was sonicated for 10 min and then added into a 100 mL glass vial with ethanol (40 mL). The vial was placed in an oven at 100 °C for 8 h, during which time a yellow suspension was formed. The Bi-NU-901 powder was soaked in DMF (25 mL), and the solvent was replaced every 2 h over a 6 h period. During each solvent exchange, the material was purified by density separation.[52]

Activation of Bi-NU-901. The Bi-NU-901 crystals were then soaked in ethanol (25 mL) twice for 2 h followed by soaking overnight in ethanol. The ethanol-containing samples were activated by supercritical CO_2 drying over a period of 8 h.[53] In this method, the liquid CO_2 was purged under positive pressure for 4 min every 2 h. Supercritical CO_2 drying (SCD) was performed with a TousimisTM Samdri PVT-30 critical point dryer. Throughout the process, the rate of purging was maintained below the rate of filling. Following the final exchange, the temperature was increased to 40 °C (above the critical temperature for CO_2), and the chamber was slowly vented over a period of 15 h at a rate of 0.1 cc/min. Bi-NU-901 crystals were then transferred to a preweighted sorption analysis tube to collect N_2 isotherms.

Characterization of Bi-NU-901. Powder X-ray diffraction data were collected at room temperature on a STOE-STADI-P powder diffractometer at Northwestern University's IMSERC facility equipped with an asymmetric curved germanium monochromator (Cu Kα1 radiation, $\lambda = 1.54056$ Å) and a one-dimensional silicon strip detector (MYTHEN2 1K from DECTRIS). The line-focused Cu X-ray tube was operated at 40 kV and 40 mA. Powder samples were packed in 3 mm metallic masks and sandwiched between polyimide tape. Intensity data for 2θ from 2° to 41° were collected over a period of 7 min. Prior to measurement, the instrument was calibrated against a NIST silicon standard (640d).

X-ray photoelectron spectroscopy (XPS) measurements were carried out at the KECK-II/NUANCE facility at NU on a Thermo Scientific ESCALAB 250 Xi (Al Kα radiation, $h\nu$ = S5, 1486.6 eV) equipped with an electron flood gun. XPS data were analyzed using Thermo Scientific Advantage Data System software, and all spectra were referenced to the C 1s peak (284.8 eV).

Scanning electron microscopy (SEM) images were collected on a Hitachi SU8030 FE-SEM (Dallas, TX) microscope at Northwestern University's EPIC/NUANCE facility. Before imaging, samples were coated with OsO_4 to ~10 nm thickness in a Denton Desk III TSC Sputter Coater (Moorestown, NJ).

The scanning transmission electron microscope (STEM) experiments were performed on a JEOL Cs-corrected ARM 200 kV (JEOL, Ltd., Akishima, Tokyo, Japan) equipped with a cold field-emission source that generates a nominal 0.1 nm probe size under standard operating conditions. The ARM 200 was operated under low dose conditions to minimize the electron beam damage. All images were acquired in the high angle annular dark field (HAADF) or Z-contrast imaging mode. The samples were prepared by drop casting the mixture of the Bi-NU-901 MOF and ethanol onto the 200-mesh copper TEM grid with lacy carbon film.

N_2 adsorption−desorption isotherms were collected at 77 K on a Micromeritics Tristar II 3020 (Micromeritics, Norcross, GA). The data points between 0.04 and 0.15 P/P_0 were chosen for apparent BET surface area calculation to minimize the error for consistency criteria ($R^2 = 0.9999$).

Thermogravimetric analysis (TGA) was performed at Northwestern University's Materials Characterization and Imaging facility using a TGA/DCS 1 system (Mettler-Toledo AG, Schwerzenbach, Switzerland) with STARe software. Samples were heated from 25 to 650 °C at a rate of 10 °C/min under a constant flow of N_2. An additional spectrum was collected under ambient conditions and following the same protocols.

ICP-OES was performed on a computer-controlled (QTEGRA software) Thermo iCap7600 ICP-OES (Thermo Fisher Scientific, Waltham, MA, USA) operating in axial view and equipped with a CETAC 520 autosampler (Omaha, NE, USA). Each sample was acquired using 5 s visible exposure time and 15 s UV exposure time, running 3 replicates. The spectral lines selected for analysis were: Bi (223.061, 306.770, 190.234 nm) and Zr (339.198, 343.823, 327.305, 349.621 nm).

CT Imaging. In preparation for CT imaging, quantification of Bi and Zr samples was accomplished using ICP-OES of acid-digested samples. Specifically, samples were digested in concentrated trace nitric acid (>69%, Thermo Fisher Scientific, Waltham, MA, USA) and placed at 65 °C for at least 3 h to allow for complete sample digestion. Ultrapure H_2O (18.2 MΩ·cm) was added to produce a final solution of 3.0% nitric acid (v/v) in a total sample volume of 7 mL. Quantitative standards consisting of 30, 20, 10, 4, 2, and 1 ppm were made using a 1000 mg/L bismuth or 1000 mg/L zirconium standard in 3.0% nitric acid (v/v) in a total sample volume of 50 mL.

CT images were acquired at Northwestern University's Center for Advanced Molecular Imaging (CAMI) with a preclinical micro PET/CT imaging system, Mediso nanoScan scanner (Mediso-USA, Boston, MA). Data were acquired with 2.17 magnification, 33 μm focal spot, and 1 × 1 binning, with 720 projection views over a full circle, with a 300 ms exposure time. Three images were acquired, using 35 kV, 50 kV, and 70 kV. The projection data were reconstructed with a voxel size of 68 μm using filtered (Butterworth filter) back-projection software from Mediso. The reconstructed data were analyzed in Amira 6.5 (FEI, Houston, TX). Regions of interest were identified for each sample at each energy. The mean image intensity, in Hounsfield Units, was used in the statistical analysis, and the data were normalized to a 1% agarose solution, in which all the samples were suspended.

■ RESULTS AND DISCUSSION

The atomic structure of Bi-NU-901 was simulated based on a combination of the crystal structure of Zr-NU-901 and a modeled $[Bi_6O_4(OH)_4(NO_3)_6(H_2O)](H_2O)$ node. The bulk phase purity of Bi-NU-901 was confirmed by comparing the experimental powder X-ray diffraction (PXRD) pattern with a simulated pattern of Bi-NU-901 and an experimental pattern of Zr-NU-901 (Figure 2a). The *scu* topology of the Bi-NU-901 phase features microporous diamond-shaped 1D channels formed by the coordination of Bi_6 nodes to eight tetratopic H_4TBAPy linkers. Nitrogen adsorption−desorption isotherms collected for activated samples of Bi-NU-901 show a type I isotherm, consistent with the microporous structure of the Bi-NU-901 phase, featuring microporous diamond-shaped 1D channels formed by the coordination of Bi_6 nodes to eight tetratopic H_4TBAPy linkers. Nitrogen adsorption−desorption isotherms collected for activated samples of Bi-NU-901 show a type I isotherm, which supports the structure of Bi-NU-901 and which is also seen in the pore size distribution (Figure 2c). The density functional theory (DFT) calculated pore size distribution revealed one pore with a diameter of ~11 Å, which corresponds closely to that of Zr-NU-901 (~12 Å). An average Brunauer−Emmett−Teller (BET) surface area of 320 m^2/g was calculated for the material. The Bi-NU-901 phase

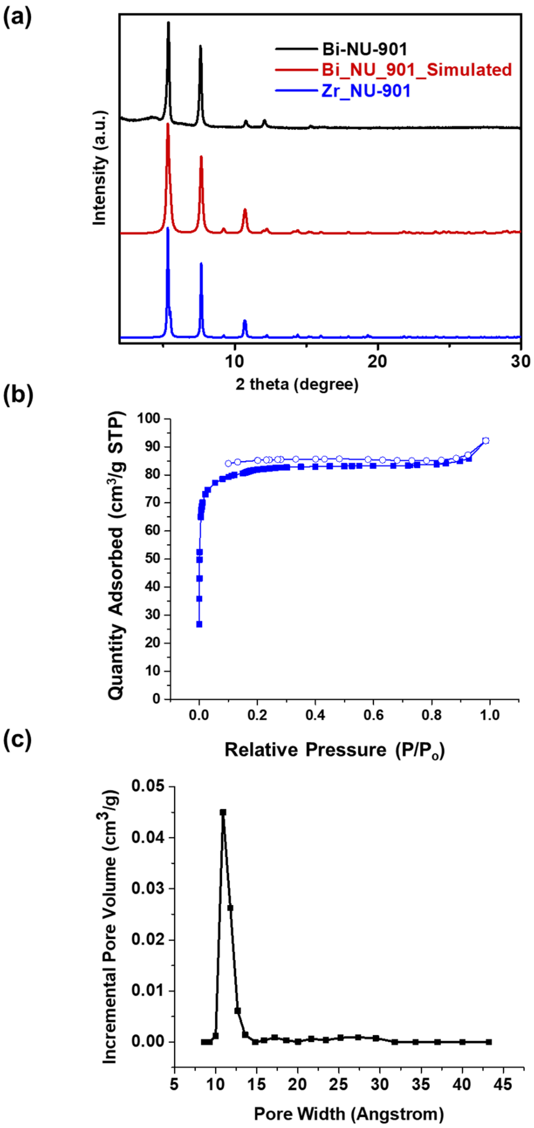

Figure 2. (a) Experimental PXRD pattern of Bi-NU-901, in agreement with the simulated pattern of Bi-NU-901 PXRD. (b) N_2 isotherms of Bi-NU-901 based on the volume and (c) pore size distribution of Bi-NU-901 calculated by the DFT model.

demonstrated no change in crystallinity or morphology following supercritical CO_2 drying as evidenced by powder X-ray diffraction (PXRD) and scanning electron microscopy images (Figures S4 and S5).

The determined *scu* topology was further supported by scanning transmission electron microscopy (STEM) images of Bi-NU-901 from which the *d*-spacing between metal nodes was calculated (Figure 3). The experimental distance between the nodes on the (001) plane was measured from the fringe spacing in the image and the associated spots in the Fourier transform to be ~15.43 Å, aligning closely with the 15.06 Å *d*-spacing calculated from the simulated Bi-NU-901 (001) plane. X-ray photoelectron spectroscopy (XPS) (Figure S1) confirmed the expected +3 valence of bismuth ions in the MOF node, and the Bi-NU-901 thermal stability was tested using thermogravimetric analysis (TGA) (Figure S3). As revealed by scanning electron microscopy (SEM), Bi-NU-901 crystals exhibit an average size of ~7.0 μm. (Figure 2b). Based upon these results and previously reported hexanuclear, 8-connected MOFs,[54−56] we propose this structure as $Bi_6(\mu_3\text{-}OH)_8(HCO_2)_2(TBAPy)_2$.

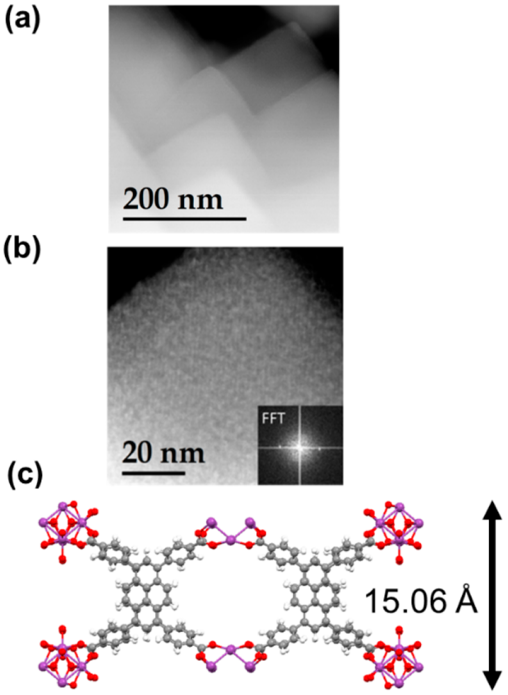

Figure 3. (a) High-angle annular dark-field (HAADF) STEM image at 200 nm and (b) at 20 nm. Inset: Fourier transform of the Bi-NU-901 sample. (c) View down the *b*-axis of the simulated Bi-NU-901 MOF. The (001) distance is shown by the black arrow.

X-ray computed tomography (CT) measurements were conducted using newly synthesized Bi-NU-901. All imaging samples were prepared by dispersing Bi-NU-901 in a 1% agarose solution, and images were obtained at varying concentrations from 3.25 to 30 mM. CT images were obtained at three different X-ray tube voltages, 35 kV, 50 kV, and 70 kV. For comparison, CT images were also collected of Zr-NU-901, the Zr-based analogue of Bi-NU-901 with the same topology, and idixanol, a commercially available iodinated contrast agent. Inductively coupled plasma optical emission spectroscopy (ICP-OES) was used to determine the mass % of the attenuating element within the MOF contrast materials, and all imaging samples were prepared with uniform concentrations of the X-ray attenuating element (Bi/Zr/I), based upon the ICP-OES results. Under all X-ray voltages, Bi-NU-901 outperforms each of the examined CT contrast agents as demonstrated by the plots of X-ray attenuation (HU) against the concentration of the respective heavy element. Notably, at 30 kV and a concentration of 30 mM, the Bi-NU-901 sample yields 14 times better contrast than idixanol, a commonly used commercial CT contrast agent (Figure 4a). At 70 kV, closer to the energies used to image humans in clinical settings, the enhancement in attenuation of the bismuth-based MOF against idixanol is 7 times better (Figure 4b). The Bi-NU-901 is 6.5 times better than the analogous Zr-NU-901 at both energies (Figure 4a, 4b), presumably because of bismuth's atomic properties which allow the atoms to attenuate X-rays easily, based upon its atomic mass and high *k*-edge value.

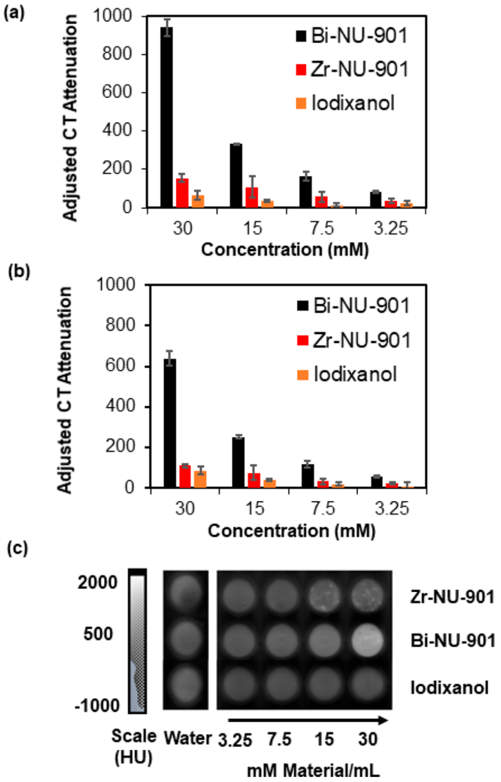

Figure 4. (a) X-ray attenuation as a function of [Bi/Zr/I] for Bi-NU-901, Zr-NU-901, and Iodixanol at 35 kV. (b) X-ray attenuation as a function of [Bi/Zr/I] for Bi-NU-901, Zr-NU-901, and Iodixanol at 70 kV. All data are included in the SI (Figure S6). (c) Coronal CT images of Zr-NU-901, Bi-NU-901, and Iodixanol dispersed in a 1% agarose solution.

In vivo examination of the cellular fate, material properties, and safety is invaluable for any new biomaterial. We plan to investigate how the size, charge, and morphology of this nanomaterial may affect MOF functionality and cell viability *in vitro*.[57,58] Toward this end, an initial stability test was undertaken, and the Bi-NU-901 MOF particles were exposed to a 1×PBS (phosphate-buffered saline; pH = 7.4) buffer solution for 24 h. The crystallinity and morphology of the MOF particles remained stable, as confirmed by both PXRD and SEM data (Figure S7). We hypothesize that, like other nanomaterials tested *in vivo*, these particles may accumulate in mononuclear phagocyte systems such as the spleen and liver once inside the body.[59] This leads us to believe that surface functionalization of the MOF with targeting groups[60] may be necessary to prevent facile opsonization; however, our first area of interest is in decreasing the size of the MOF particles from the micron regime to below 100 nm.[61] We will adapt similar protocols to nanosize this MOF, as previously reported, and plan to report this in due time.[62,63] Nanosizing this Bi-NU-901 MOF will also allow us to investigate how the size, shape, and stability of the material may affect cells *in vitro*.[64]

■ CONCLUSION

In summary, we report the synthesis of a new cluster-based bismuth MOF and tested its ability *in vitro* to effectively act as new contrast media for CT. The Bi_6 nodes and tetratopic pyrene-based linkers assembled into the 8-connected *scu* topology. Characterization strategies including PXRD, TEM, SEM, N_2 isotherm measurements, and calculated DFT pore size distribution further support the determined framework structure. To assess the ability of this MOF to serve as a CT contrast agent, we collected CT images of Bi-NU-901, the zirconium analogue, Zr-NU-901, and a commercially available CT contrast agent, idixanol. At each of the three X-ray voltages tested, Bi-NU-901 outperformed all other contrast agents. Therefore, much less material would be needed for clinical scans as compared to contrast agents in current use. It is well documented in the literature that some materials at the nanoscale regime do not readily circulate to extravascular space or experience swift renal clearance, so synthesizing the Bi-NU-901 MOF on the nanoscale size regime would be advantageous for intravenous delivery.[61,65] Our investigation could expand the role MOFs play in imaging applications and may lead to designing more effective nanomaterials for contrast media in the future. We are optimistic that MOFs constructed from heavy elements hold promise in improved CT contrast media, particularly since the role of dual-energy CT imaging[66−68] continues to increase, and we envision that their investigation in the synthesis of CT agents with specific targeting or biodistribution profiles may be quite useful.[69,70]

■ ASSOCIATED CONTENT

Ⓢ Supporting Information

The Supporting Information is available free of charge on the ACS Publications website at DOI: 10.1021/acsabm.8b00778.

Materials and experimental methods, characterization data, computed tomography (CT) data, and stability data (PDF)

■ AUTHOR INFORMATION

Corresponding Author

*E-mail: o-farha@northwestern.edu.

ORCID

Lee Robison: 0000-0002-7419-4499
Lin Zhang: 0000-0001-5853-3107
Riki J. Drout: 0000-0002-3511-7597
Peng Li: 0000-0002-4273-4577
Hyunho Noh: 0000-0003-3136-1004
B. Layla Mehdi: 0000-0002-8281-9524
Vinayak P. Dravid: 0000-0002-6007-3063
Timur Islamoglu: 0000-0003-3688-9158
Omar K. Farha: 0000-0002-9904-9845

Author Contributions

#L.R. and L.Z. contributed equally. The manuscript was written through contributions of all authors. All authors have given approval to the final version of the manuscript.

Notes

The authors declare no competing financial interest.

■ ACKNOWLEDGMENTS

The authors gratefully acknowledge financial support from the U.S. Department of Energy, National Nuclear Security Administration under Award Number DE-NA0003763. The authors appreciate financial support from Toyota. This work made use of the Center for Advanced Molecular Imaging generously supported by NCI CCSG P30 CA060553 awarded to the Robert H. Lurie Comprehensive Cancer Center. Use was made of the IMSERC X-ray Facility at Northwestern University, which has received support from the Soft and Hybrid Nanotechnology Experimental (SHyNE) Resource (NSF ECCS-1542205); the State of Illinois and International Institute for Nanotechnology (IIN). Elemental analysis was performed at the Northwestern University Quantitative Bio-element Imaging Center. This work also made use of the EPIC facility of Northwestern University's NUANCE Center, which has received support from the Soft and Hybrid Nanotechnology Experimental (SHyNE) Resource (NSF ECCS-1542205); the MRSEC program (NSF DMR-1720139) at the Materials Research Center; the International Institute for Nanotechnology (IIN); the Keck Foundation; and the State of Illinois, through the IIN. L.R. gratefully acknowledges the NSF Graduate Research Fellowship. L.Z. gratefully acknowledges a Graduate Student International Exchange Fellowship from Nanjing Tech University and a Graduate Fellowship from Nanjing Tech University. R.J.D. gratefully acknowledges an International Institute for Nanotechnology (IIN) Graduate Student Ryan Fellowship. The authors would also like to thank Dr. Haoyuan Chen for initial simulations of bismuth MOF models.

■ REFERENCES

(1) Hsieh, J. *Computed Tomography - Principles, Design, Artifacts and Recent Advances* **2009**, 556.

(2) Moyal, A. E. *Nationwide Evaluation of X-Ray Trends Tabulation and Graphical Summary of the 1999 Dental Radiography Survey*; 1999; pp 1−83.

(3) Lusic, H.; Grinstaff, M. W. X-Ray Computed Tomography Contrast Agents. *Chem. Rev.* **2013**, *113* (3), 1641−1666.

(4) Bottinor, W.; Polkampally, P.; Jovin, I. Adverse Reactions to Iodinated Contrast Media. *Int. J. Angiol.* **2013**, *22* (3), 149−154.

(5) Mruk, B. Renal Safety of Iodinated Contrast Media Depending on Their Osmolarity − Current Outlooks. *Polym. J. Radiol.* **2016**, *81*, 157−165.

(6) Ng, C. S.; Kalva, S. P.; Gunnarsson, C.; Ryan, M. P.; Baker, E. R.; Mehta, R. L. Risk of Renal Events Following Intravenous Iodinated Contrast Material Administration Among Inpatients Admitted with Cancer a Retrospective Hospital Claims Analysis. *Cancer Imaging* **2018**, *18*, 30.

(7) Pasternak, J. J.; Williamson, E. E. Clinical Pharmacology, Uses, and Adverse Reactions of Iodinated Contrast Agents: A Primer for the Non-Radiologist. *Mayo Clin. Proc.* **2012**, *87* (4), 390−402.

(8) Widmark, J. M. Imaging-Related Medications: A Class Overview. *Proc. (Bayl Univ Med. Cent)* **2007**, *20* (4), 408−417.

(9) Yu, S.-B.; Watson, A. D. Metal-Based X-ray Contrast Media. *Chem. Rev.* **1999**, *99* (9), 2353−2378.

(10) Yang, Y.; Ouyang, R.; Xu, L.; Guo, N.; Li, W.; Feng, K.; Ouyang, L.; Yang, Z.; Zhou, S.; Miao, Y. Review: Bismuth Complexes:

Synthesis and Applications in Biomedicine. *J. Coord. Chem.* **2015**, *68* (3), 379−397.

(11) Malfertheiner, P.; Bazzoli, F.; Delchier, J.-C.; Celiñski, K.; Giguère, M.; Rivière, M.; Mégraud, F. Helicobacter Pylori Eradication with a Capsule Containing Bismuth Subcitrate Potassium, Metronidazole, and Tetracycline Given with Omeprazole Versus Clarithromycin-Based Triple Therapy: A Randomised, Open-Label, Non-Inferiority, Phase 3 Trial. *Lancet* **2011**, *377* (9769), 905−913.

(12) Rabin, O.; Manuel Perez, J.; Grimm, J.; Wojtkiewicz, G.; Weissleder, R. An X-ray Computed Tomography Imaging Agent Based on Long-Circulating Bismuth Sulphide Nanoparticles. *Nat. Mater.* **2006**, *5*, 118−122.

(13) Naha, P. C.; Al Zaki, A.; Hecht, E.; Chorny, M.; Chhour, P.; Blankemeyer, E.; Yates, D. M.; Witschey, W. R. T.; Litt, H. I.; Tsourkas, A.; Cormode, D. P. Dextran Coated Bismuth−Iron Oxide Nanohybrid Contrast Agents for Computed Tomography and Magnetic Resonance Imaging. *J. Mater. Chem. B* **2014**, *2* (46), 8239−8248.

(14) Hernández-Rivera, M.; Kumar, I.; Cho, S. Y.; Cheong, B. Y.; Pulikkathara, M. X.; Moghaddam, S. E.; Whitmire, K. H.; Wilson, L. J. High-Performance Hybrid Bismuth−Carbon Nanotube Based Contrast Agent for X-ray CT Imaging. *ACS Appl. Mater. Interfaces* **2017**, *9* (7), 5709−5716.

(15) Perera, V. S.; Hao, J.; Gao, M.; Gough, M.; Zavalij, P. Y.; Flask, C.; Basilion, J. P.; Huang, S. D. Nanoparticles of the Novel Coordination Polymer KBi(H2O)2[Fe(CN)6]·H2O As a Potential Contrast Agent for Computed Tomography. *Inorg. Chem.* **2011**, *50* (17), 7910−7912.

(16) Zhang, G.; Naha, P. C.; Gautam, P.; Cormode, D. P.; Chan, J. M. W. Water-Dispersible Bismuth−Organic Materials with Computed Tomography Contrast Properties. *ACS Appl. Bio Mater.* **2018**, *1* (6), 1918−1926.

(17) Jakhmola, A.; Anton, N.; Vandamme, T. F. Inorganic Nanoparticles Based Contrast Agents for X-ray Computed Tomography. *Adv. Healthcare Mater.* **2012**, *1* (4), 413−431.

(18) Lee, N.; Choi, S. H.; Hyeon, T. Nano-Sized CT Contrast Agents. *Adv. Mater.* **2013**, *25* (19), 2641−2660.

(19) Kim, D.; Park, S.; Lee, J. H.; Jeong, Y. Y.; Jon, S. Antibiofouling Polymer-Coated Gold Nanoparticles as a Contrast Agent for in Vivo X-ray Computed Tomography Imaging. *J. Am. Chem. Soc.* **2007**, *129* (24), 7661−7665.

(20) Liu, Y.; Ai, K.; Liu, J.; Yuan, Q.; He, Y.; Lu, L. A High-Performance Ytterbium-Based Nanoparticulate Contrast Agent for In Vivo X-Ray Computed Tomography Imaging. *Angew. Chem.* **2012**, *124* (6), 1466−1471.

(21) Cole, L. E.; Ross, R. D.; Tilley, J. M.; Vargo-Gogola, T.; Roeder, R. K. Gold Nanoparticles as Contrast Agents in X-Ray Imaging and Computed Tomography. *Nanomedicine* **2015**, *10* (2), 321−341.

(22) Oh, M. H.; Lee, N.; Kim, H.; Park, S. P.; Piao, Y.; Lee, J.; Jun, S. W.; Moon, W. K.; Choi, S. H.; Hyeon, T. Large-Scale Synthesis of Bioinert Tantalum Oxide Nanoparticles for X-ray Computed Tomography Imaging and Bimodal Image-Guided Sentinel Lymph Node Mapping. *J. Am. Chem. Soc.* **2011**, *133* (14), 5508−5515.

(23) Massich, M. D.; Giljohann, D. A.; Schmucker, A. L.; Patel, P. C.; Mirkin, C. A. Cellular Response of Polyvalent Oligonucleotide−Gold Nanoparticle Conjugates. *ACS Nano* **2010**, *4* (10), 5641−5646.

(24) Cormode, D. P.; Naha, P. C.; Fayad, Z. A. Nanoparticle Contrast Agents for Computed Tomography: A Focus on Micelles. *Contrast Media Mol. Imaging* **2014**, *9* (1), 37−52.

(25) Mukundan, S.; Ghaghada, K. B.; Badea, C. T.; Kao, C.-Y.; Hedlund, L. W.; Provenzale, J. M.; Johnson, G. A.; Chen, E.; Bellamkonda, R. V.; Annapragada, A. A Liposomal Nanoscale Contrast Agent for Preclinical CT in Mice. *AJR, Am. J. Roentgenol.* **2006**, *186* (2), 300−307.

(26) Zheng, J.; Liu, J.; Dunne, M.; Jaffray, D. A.; Allen, C. In Vivo Performance of a Liposomal Vascular Contrast Agent for CT and MR-Based Image Guidance Applications. *Pharm. Res.* **2007**, *24* (6), 1193−1201.

(27) de Vries, A.; Custers, E.; Lub, J.; van den Bosch, S.; Nicolay, K.; Grüll, H. Block-Copolymer-Stabilized Iodinated Emulsions for Use as CT Contrast Agents. *Biomaterials* **2010**, *31* (25), 6537−6544.

(28) Fu, Y.; Nitecki, D. E.; Maltby, D.; Simon, G. H.; Berejnoi, K.; Raatschen, H.-J.; Yeh, B. M.; Shames, D. M.; Brasch, R. C. Dendritic Iodinated Contrast Agents with PEG-Cores for CT Imaging: Synthesis and Preliminary Characterization. *Bioconjugate Chem.* **2006**, *17* (4), 1043−1056.

(29) Li, H.; Eddaoudi, M.; O'Keeffe, M.; Yaghi, O. M. Design and Synthesis of an Exceptionally Stable and Highly Porous Metal-Organic Framework. *Nature* **1999**, *402* (6759), 276−279.

(30) Li, J. R.; Kuppler, R. J.; Zhou, H. C. Selective Gas Adsorption and Separation in Metal-Organic Frameworks. *Chem. Soc. Rev.* **2009**, *38* (5), 1477−1504.

(31) Eddaoudi, M.; Kim, J.; Rosi, N.; Vodak, D.; Wachter, J.; O'Keeffe, M.; Yaghi, O. M. Systematic Design of Pore Size and Functionality in Isoreticular MOFs and Their Application in Methane Storage. *Science* **2002**, *295* (5554), 469−472.

(32) Horcajada, P.; Chalati, T.; Serre, C.; Gillet, B.; Sebrie, C.; Baati, T.; Eubank, J. F.; Heurtaux, D.; Clayette, P.; Kreuz, C.; Chang, J. S.; Hwang, Y. K.; Marsaud, V.; Bories, P. N.; Cynober, L.; Gil, S.; Ferey, G.; Couvreur, P.; Gref, R. Porous Metal-Organic-Framework Nanoscale Carriers as a Potential Platform for Drug Delivery and Imaging. *Nat. Mater.* **2010**, *9* (2), 172−178.

(33) Chen, Y.; Li, P.; Modica, J. A.; Drout, R. J.; Farha, O. K. Acid-Resistant Mesoporous Metal−Organic Framework toward Oral Insulin Delivery: Protein Encapsulation, Protection, and Release. *J. Am. Chem. Soc.* **2018**, *140* (17), 5678−5681.

(34) Teplensky, M. H.; Fantham, M.; Li, P.; Wang, T. C.; Mehta, J. P.; Young, L. J.; Moghadam, P. Z.; Hupp, J. T.; Farha, O. K.; Kaminski, C. F.; Fairen-Jimenez, D. Temperature Treatment of Highly Porous Zirconium-Containing Metal−Organic Frameworks Extends Drug Delivery Release. *J. Am. Chem. Soc.* **2017**, *139* (22), 7522−7532.

(35) Lee, J.; Farha, O. K.; Roberts, J.; Scheidt, K. A.; Nguyen, S. T.; Hupp, J. T. Metal-Organic Framework Materials as Catalysts. *Chem. Soc. Rev.* **2009**, *38* (5), 1450−1459.

(36) deKrafft, K. E.; Boyle, W. S.; Burk, L. M.; Zhou, O. Z.; Lin, W. Zr- and Hf-Based Nanoscale Metal-Organic Frameworks as Contrast Agents for Computed Tomography. *J. Mater. Chem.* **2012**, *22* (35), 18139−18144.

(37) McKinlay, A. C.; Morris, R. E.; Horcajada, P.; Férey, G.; Gref, R.; Couvreur, P.; Serre, C. BioMOFs: Metal−Organic Frameworks for Biological and Medical Applications. *Angew. Chem., Int. Ed.* **2010**, *49* (36), 6260−6266.

(38) Li, P.; Modica, J. A.; Howarth, A. J.; Vargas, L. E.; Moghadam, P. Z.; Snurr, R. Q.; Mrksich, M.; Hupp, J. T.; Farha, Omar K. Toward Design Rules for Enzyme Immobilization in Hierarchical Mesoporous Metal-Organic Frameworks. *Chem.* **2016**, *1* (1), 154−169.

(39) Xiao, J.; Zhu, Y.; Huddleston, S.; Li, P.; Xiao, B.; Farha, O. K.; Ameer, G. A. Copper Metal−Organic Framework Nanoparticles Stabilized with Folic Acid Improve Wound Healing in Diabetes. *ACS Nano* **2018**, *12* (2), 1023−1032.

(40) Rieter, W. J.; Taylor, K. M. L.; An, H.; Lin, W.; Lin, W. Nanoscale Metal−Organic Frameworks as Potential Multimodal Contrast Enhancing Agents. *J. Am. Chem. Soc.* **2006**, *128* (28), 9024−9025.

(41) Lu, W.; Wei, Z.; Gu, Z.-Y.; Liu, T.-F.; Park, J.; Park, J.; Tian, J.; Zhang, M.; Zhang, Q.; Gentle, T., III; Bosch, M.; Zhou, H.-C. Tuning the Structure and Function of Metal−Organic Frameworks Via Linker Design. *Chem. Soc. Rev.* **2014**, *43* (16), 5561−5593.

(42) Horcajada, P.; Chalati, T.; Serre, C.; Gillet, B.; Sebrie, C.; Baati, T.; Eubank, J. F.; Heurtaux, D.; Clayette, P.; Kreuz, C.; Chang, J.-S.; Hwang, Y. K.; Marsaud, V.; Bories, P.-N.; Cynober, L.; Gil, S.; Férey, G.; Couvreur, P.; Gref, R. Porous Metal−Organic-Framework Nanoscale Carriers as a Potential Platform for Drug Delivery and Imaging. *Nat. Mater.* **2010**, *9*, 172−178.

(43) Kung, C.-W.; Wang, T. C.; Mondloch, J. E.; Fairen-Jimenez, D.; Gardner, D. M.; Bury, W.; Klingsporn, J. M.; Barnes, J. C.; Van

Duyne, R.; Stoddart, J. F.; Wasielewski, M. R.; Farha, O. K.; Hupp, J. T. Metal−Organic Framework Thin Films Composed of Free-Standing Acicular Nanorods Exhibiting Reversible Electrochromism. *Chem. Mater.* **2013**, *25* (24), 5012−5017.

(44) Noh, H.; Kung, C.-W.; Islamoglu, T.; Peters, A. W.; Liao, Y.; Li, P.; Garibay, S. J.; Zhang, X.; DeStefano, M. R.; Hupp, J. T.; Farha, O. K. Room Temperature Synthesis of an 8-Connected Zr-Based Metal−Organic Framework for Top-Down Nanoparticle Encapsulation. *Chem. Mater.* **2018**, *30* (7), 2193−2197.

(45) Janib, S. M.; Moses, A. S.; MacKay, J. A. Imaging and Drug Delivery Using Theranostic Nanoparticles. *Adv. Drug Delivery Rev.* **2010**, *62* (11), 1052−1063.

(46) Savage, M.; Yang, S.; Suyetin, M.; Bichoutskaia, E.; Lewis, W.; Blake, A. J.; Barnett, S. A.; Schröder, M. A Novel Bismuth-Based Metal−Organic Framework for High Volumetric Methane and Carbon Dioxide Adsorption. *Chem. - Eur. J.* **2014**, *20* (26), 8024−8029.

(47) Inge, A. K.; Köppen, M.; Su, J.; Feyand, M.; Xu, H.; Zou, X.; O'Keeffe, M.; Stock, N. Unprecedented Topological Complexity in a Metal−Organic Framework Constructed from Simple Building Units. *J. Am. Chem. Soc.* **2016**, *138* (6), 1970−1976.

(48) Köppen, M.; Beyer, O.; Wuttke, S.; Lüning, U.; Stock, N. Synthesis, Functionalisation and Post-synthetic Modification of Bismuth Metal−Organic Frameworks. *Dalton Trans.* **2017**, *46* (26), 8658−8663.

(49) Köppen, M.; Meyer, V.; Ångström, J.; Inge, A. K.; Stock, N. Solvent-Dependent Formation of Three New Bi-Metal−Organic Frameworks Using a Tetracarboxylic Acid. *Cryst. Growth Des.* **2018**, *18* (7), 4060−4067.

(50) Feyand, M.; Mugnaioli, E.; Vermoortele, F.; Bueken, B.; Dieterich, J. M.; Reimer, T.; Kolb, U.; de Vos, D.; Stock, N. Automated Diffraction Tomography for the Structure Elucidation of Twinned, Sub-micrometer Crystals of a Highly Porous, Catalytically Active Bismuth Metal−Organic Framework. *Angew. Chem., Int. Ed.* **2012**, *51* (41), 10373−10376.

(51) Wang, T. C.; Vermeulen, N. A.; Kim, I. S.; Martinson, A. B. F.; Stoddart, J. F.; Hupp, J. T.; Farha, O. K. Scalable Synthesis and Post-Modification of a Mesoporous Metal-Organic Framework Called NU-1000. *Nat. Protoc.* **2016**, *11*, 149.

(52) Farha, O. K.; Mulfort, K. L.; Thorsness, A. M.; Hupp, J. T. Separating Solids: Purification of Metal-Organic Framework Materials. *J. Am. Chem. Soc.* **2008**, *130* (27), 8598−8599.

(53) Nelson, A. P.; Farha, O. K.; Mulfort, K. L.; Hupp, J. T. Supercritical Processing as a Route to High Internal Surface Areas and Permanent Microporosity in Metal−Organic Framework Materials. *J. Am. Chem. Soc.* **2009**, *131* (2), 458−460.

(54) Alezi, D.; Peedikakkal, A. M. P.; Weseliński, Ł. J.; Guillerm, V.; Belmabkhout, Y.; Cairns, A. J.; Chen, Z.; Wojtas, Ł.; Eddaoudi, M. Quest for Highly Connected Metal−Organic Framework Platforms: Rare-Earth Polynuclear Clusters Versatility Meets Net Topology Needs. *J. Am. Chem. Soc.* **2015**, *137* (16), 5421−5430.

(55) Xue, D.-X.; Cairns, A. J.; Belmabkhout, Y.; Wojtas, L.; Liu, Y.; Alkordi, M. H.; Eddaoudi, M. Tunable Rare-Earth fcu-MOFs: A Platform for Systematic Enhancement of CO2 Adsorption Energetics and Uptake. *J. Am. Chem. Soc.* **2013**, *135* (20), 7660−7667.

(56) Luebke, R.; Belmabkhout, Y.; Weseliński, Ł. J.; Cairns, A. J.; Alkordi, M.; Norton, G.; Wojtas, Ł.; Adil, K.; Eddaoudi, M. Versatile Rare Earth Hexanuclear Clusters for the Design and Synthesis of Highly-Connected Ftw-MOFs. *Chem. Sci.* **2015**, *6* (7), 4095−4102.

(57) Sajid, M. Toxicity of Nanoscale Metal Organic Frameworks: A Perspective. *Environ. Sci. Pollut. Res.* **2016**, *23* (15), 14805−14807.

(58) Albanese, A.; Tang, P. S.; Chan, W. C. W. The Effect of Nanoparticle Size, Shape, and Surface Chemistry on Biological Systems. *Annu. Rev. Biomed. Eng.* **2012**, *14* (1), 1−16.

(59) Blanco, E.; Shen, H.; Ferrari, M. Principles of Nanoparticle Sesign for Overcoming Biological Barriers to Drug Delivery. *Nat. Biotechnol.* **2015**, *33*, 941−951.

(60) Singh, R.; Lillard, J. W. Nanoparticle-Based Targeted Drug Delivery. *Exp. Mol. Pathol.* **2009**, *86* (3), 215−223.

(61) Majewski, M. B.; Noh, H.; Islamoglu, T.; Farha, O. K NanoMOFs: little crystallites for substantial applications. *J. Mater. Chem. A* **2018**, *6* (17), 7338−7350.

(62) Li, P.; Moon, S.-Y.; Guelta, M. A.; Lin, L.; Gómez-Gualdrón, D. A.; Snurr, R. Q.; Harvey, S. P.; Hupp, J. T.; Farha, O. K. Nanosizing a Metal−Organic Framework Enzyme Carrier for Accelerating Nerve Agent Hydrolysis. *ACS Nano* **2016**, *10* (10), 9174−9182.

(63) Li, P.; Klet, R. C.; Moon, S.-Y.; Wang, T. C.; Deria, P.; Peters, A. W.; Klahr, B. M.; Park, H.-J.; Al-Juaid, S. S.; Hupp, J. T.; Farha, O. K. Synthesis of Nanocrystals of Zr-Based Metal−Organic Frameworks with Csq-Net: Significant Enhancement in the Degradation of a Nerve Agent Simulant. *Chem. Commun.* **2015**, *51* (54), 10925−10928.

(64) Simon-Yarza, T.; Mielcarek, A.; Couvreur, P.; Serre, C. Nanoparticles of Metal-Organic Frameworks: On the Road to In Vivo Efficacy in Biomedicine. *Adv. Mater.* **2018**, *30* (37), 1707365.

(65) Farokhzad, O. C.; Langer, R. Impact of Nanotechnology on Drug Delivery. *ACS Nano* **2009**, *3* (1), 16−20.

(66) Goo, H. W.; Goo, J. M. Dual-Energy CT: New Horizon in Medical Imaging. *Korean J. Radiol.* **2017**, *18* (4), 555−569.

(67) McCollough, C. H.; Leng, S.; Yu, L.; Fletcher, J. G. Dual- and Multi-Energy CT: Principles, Technical Approaches, and Clinical Applications. *Radiology* **2015**, *276* (3), 637−653.

(68) Yeh, B. M.; FitzGerald, P. F.; Edic, P. M.; Lambert, J. W.; Colborn, R. E.; Marino, M. E.; Evans, P. M.; Roberts, J. C.; Wang, Z. J.; Wong, M. J.; Bonitatibus, P. J. Opportunities for New CT Contrast Agents to Maximize the Diagnostic Potential of Emerging Spectral CT Technologies. *Adv. Drug Delivery Rev.* **2017**, *113*, 201−222.

(69) Peng, C.; Qin, J.; Zhou, B.; Chen, Q.; Shen, M.; Zhu, M.; Lu, X.; Shi, X. Targeted Tumor CT Imaging Using Folic Acid-Modified PEGylated Dendrimer-Entrapped Gold Nanoparticles. *Polym. Chem.* **2013**, *4* (16), 4412−4424.

(70) Popovtzer, R.; Agrawal, A.; Kotov, N. A.; Popovtzer, A.; Balter, J.; Carey, T. E.; Kopelman, R. Targeted Gold Nanoparticles Enable Molecular CT Imaging of Cancer. *Nano Lett.* **2008**, *8* (12), 4593−4596.

DOI: 10.1021/acsabm.8b00778
ACS Appl. Bio Mater. XXXX, XXX, XXX−XXX